Relationship between Residual Stress of Dissimilar Metal Welding and Stress Corrosion Cracking of Alloy 600 Nozzle in Bottom Mounted Instrumentation of PWR

Sung-Woo Kim [a*], Hong-Pyo Kim [a], Jae-Uk Jeong [b], Yoon-Suk Chang [c]
[a]*Nucl. Mater. Res. Div., Korea Atomic Energy Res. Inst., 1045 Daedeokdaero, Yuseong-gu, Daejeon 305-353, Korea*
[b]*School of Mech. Eng., Sungkyunkwan Univ., 300 Chunchun-dong, Jangan-gu, Suwon, Kyunggi-do 440-746, Korea*
[c]*Dept. of Nucl. Eng., Kyunghee Univ., Seocheon-dong, Giheung-gu, Yongin, Kyunggi-do 446-701, Korea*
[*]*Corresponding author: kimsw@kaeri.re.kr*

1. Introduction

One of the main concerns of the dissimilar metal weld (DMW) parts in a pressurized water reactor (PWR) is a tensile stress generated by welding or cold working. Under an abnormal welding condition or without a sufficient post-heat treatment, a high tensile stress can be persistent after welding, leading to cracking of the components even in a short-term operation. Under the circumstances, significant efforts have been recently devoted to evaluate the stress generation in the DMW parts during welding [1,2] and to investigate the effect of the residual stress on the stress corrosion cracking (SCC) of weld metals [3,4]. However, there is very limited literature on the relationship between the residual stress and the primary water SCC (PWSCC) of the thick wall penetration nozzle of Alloy 600 in the PWR.

In this work, the SCC behavior of the bottom mounted instrumentation (BMI) mockup and its dependence on the residual stress of welding are investigated by a finite element analysis (FEA) and an SCC acceleration test in an acidic solution to understand the field experience of PWSCC, especially, of the Alloy 600 nozzle in the PWR.

2. Experimentals

The BMI penetration mockup was constructed from Alloy 600 pipe (Schmidt-Clemens GmbH Co., Heat no. 92775) as BMI nozzle, SA508 support (Doosan Heavy Industries and Construction Co. Ltd., Gr.3 Cl.1) as reactor pressure vessel (RPV) and Alloy 182 weld metal (ESAB SeAH Co., ENiCrFe-3). Prior to welding, all the nozzles were heat-treated at 1150 ^{o}C for 15 min and then sensitized at 600 ^{o}C for 10 h. The dimensions of the mockups are listed in Table I: the main variable in the specimen design was the nozzle wall thickness. The DMW was performed using a shield metal arc welding (SMAW) according to the welding procedure specification (WPS) qualified under ASME Section IX.

The finite element model for welding process simulation in this work was an axis-symmetric model with mesh generation using the commercial pre- and post-processor, I-DEAS. The detailed procedures of the FEA and all input parameters such as thermal and mechanical properties of materials, and thermal and mechanical boundary conditions were provided in the previous work [5].

SCC acceleration tests of the BMI penetration mockups were carried out in 1 M sodium tetrathionate ($Na_2S_4O_6$) solution at room temperature. The tests were interrupted at exposure times of 1, 2 and 7 days in the solution, and the inner surface of the nozzles was non-destructively examined for cracking by an eddy current test (ECT) with a magnetic biased/plus point motorized rotating probe coil (MRPC, Zetec Inc.) at 300 kHz. After 7 days exposure, the nozzles were pulled out of the mockups and then destructively examined for cracking by a penetration test (PT) and by a scanning electron microscope (SEM, Jeol JSM-6360).

3. Results and Discussion

Fig. 1 presents the ID changes of the nozzles with various wall thicknesses numerically calculated by FEA and experimentally measured from the mockup specimens. From the FEA of the mockup models, T4J10, T6J10 and T12J10 without the constraint, the maximum ID change of the nozzle was revealed to increase with decreasing wall thickness. The maximum ID change of the nozzle in the T4J10 mockup without the constraint (case 3) was very close to the change in the T12J33 mockup with the constraint (case 1). It was also clear that the calculated values were well consistent with those values experimentally measured from the mockup specimens.

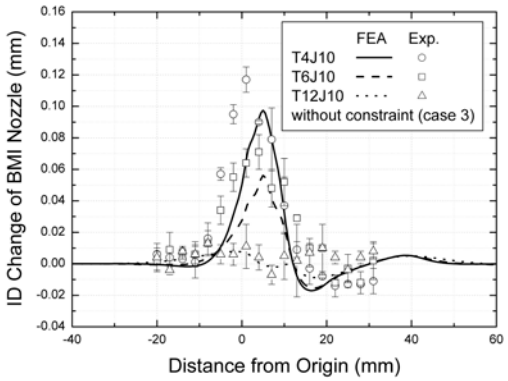

Fig. 1. ID changes of the BMI nozzles along distance from origin calculated by FEA (cases 1 and 3) and measured from the mockup specimens (case 3).

Fig. 2 depicts the residual stress distributions in the inner surface of the nozzles of the mockup models, T4J10, T6J10 and T12J10 without the constraint of the support during the DMW. It should be noted that the

residual hoop stress in the inner surface of the nozzle of the T4J10 and T6J10 mockups was expected to be tensile in the J-weld region, whereas the residual axial stress was predicted to be mainly compressive in the J-weld region but to be tensile beyond both J-weld root and face. In the case of the T12J10 mockup, only hoop stress was estimated to be tensile in the inner surface of the nozzle.

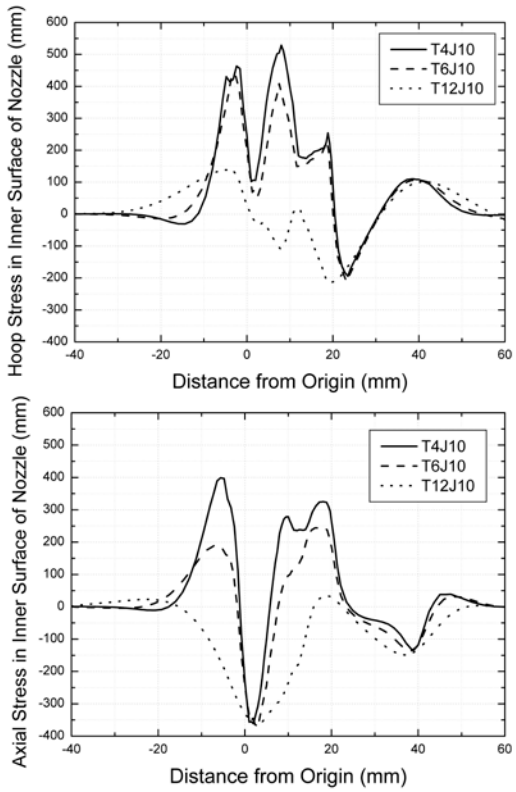

Fig. 2. Residual hoop and axial stresses in the inner surface of the BMI nozzles with various wall thicknesses calculated by FEA (case 3).

From the ECT and PT after the SCC acceleration tests, multiple axial cracks were observed in the J-weld region of all specimens while multiple circumferential cracks were found beyond the J-weld root and face of the T4J10 and T6J10 specimens. Moreover, the size of the cracks increased as the wall thickness of the nozzles decreased. Those cracks turned out to be IGSCC, propagated in an intergranular (IG) mode from the inner surface of the nozzles, as shown by SEM analysis. Fig. 3 presents the SEM micrograph of the cross section and fractured surface of one of the axial cracks in the T4J10 specimen. Multiple volumetric defects of IGA were found in the J-weld region, as well as IGSCC.

4. Conclusions

Bearing in mind that the tensile hoop stress was expected in the J-weld region whereas the tensile residual axial stress was predicted beyond both J-weld root and face by the residual stress analyses, it was reasonable to admit that the SCC behavior of the nozzle in the BMI mockup was closely related with the characteristics of the residual stress induced by the DMW.

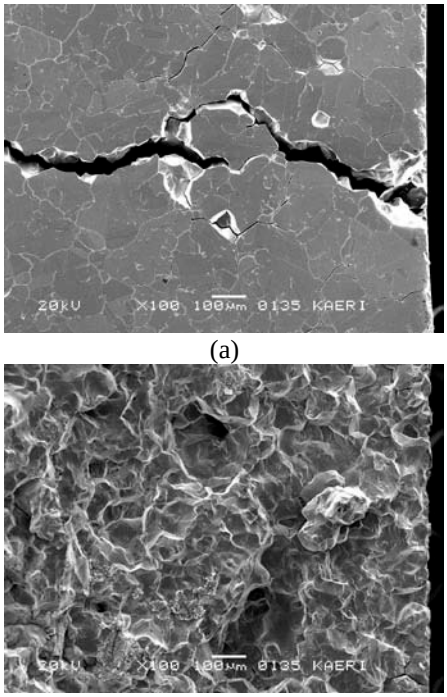

Fig. 3. . SEM micrographs of (a) the cross section and (b) fracture surface of the axial crack in the surface of the BMI nozzle from the T4J10 specimen after 7 days exposure.

REFERENCES

[1] K. Ogawa et al., Comp. Mater. Sci., Vol.45, p.1031, 2009.
[2] D. Deng et al., Comp. Mater. Sci. Vol.47, p. 398, 2009.
[3] P. Scott et al., 13th Int. Conf. on Env. Deg. of Mater. in Nucl. Power Syst., Aug. 19-23, 2007, Whistler, BC.
[4] F. Vaillant et al., *ibid.*
[5] S.C. Yu et al., ASME Pressure Vessels and Piping Div. Conf., July 27-31, 2008, Chicago, IL.

Table I: Dimensions of the components in the mockups (mm)

Specimen	Alloy 600 BMI nozzle			SA508 Support			
	ID	Thickness	Length	J-groove width	J-groove depth	Length	OD
T12J33	15.5	12	100	33	33	40	150
T4J10	15.5	4	100	10	10	40	150
T6J10	15.5	6	100	10	10	40	150
T12J10	15.5	12	100	10	10	40	150